Journal of Iron and Steel Research, International 24 (2017) 177—183

Contents lists available at ScienceDirect

Journal of Iron and Steel Research, International

journal homepage: www.chinamet.cn

Effects of Ni on austenite stability and fracture toughness in high Co-Ni secondary hardening steel

Chen-chong Wang, Chi Zhang*, Zhi-gang Yang

Key Laboratory of Advanced Materials of Ministry of Education, School of Materials Science and Engineering, Tsinghua University, Beijing 100084, China

ARTICLE INFO

Key words:
Austenite stability
Transformation-induced plasticity
Fracture toughness
Diffusion kinetic
Element distribution

ABSTRACT

Three kinds of high Co-Ni secondary hardening steels with different Ni contents were studied. The nanoscale austenite layers formed at the interface of matensite laths were observed. Both observation and diffusion kinetic simulation results showed that both Ni and Co did not obtain enough time to get the equilibrium content in this system. The Ni content in austenite layers decreased significantly, and Co content increased slightly with the decrease of Ni content in overall composition. The austenite stability was estimated by Olson-Cohen model, in which both chemical and mechanical driving force could be calculated by equilibrium thermodynamic and Mohr's circle methods, respectively. Simulation and mechanical test results showed that the decrease of Ni content in austenite layers would cause the change of austenite stability and decrease the fracture toughness of the steels. When the Ni content in the overall composition was lower than 7 wt. %, the Ni content in γ phase would be lower than 20 wt. %. And the simulation value of M_s^σ (stress-induced critical martensite transformation temperature) would be up to 80 °C, which was about 60 °C higher than room temperature. Based on the analysis, the Ni content in the overall composition of high Co-Ni secondary hardening steels should be higher than 8 wt. % in order to obtain a good fracture toughness.

1. Introduction

With the development of structure materials, there has been extensive interest in improving the mechanical properties of steels in the past decades[1-3]. Recently, several high Co-Ni secondary hardening steels, which had ultra-high strength and relatively high toughness, were developed[4-6]. In these steels, nanoscale carbides formed in the matrix, which led to high strength of the steel based on dispersion strengthening[7-9]. Also, much attention was paid to the nanoscale austenite layers formed at the boundary of martensite laths[10,11]. These austenite layers would probably make significant contribution to the toughness of the steel by transformation induced plasticity (TRIP) effect[12].

As a long-standing topic, TRIP effect was studied by many researchers for more than fifty years and many critical results were obtained in TRIP steels[13-15]. It is well-known that the stability of austenite is the key factor of TRIP effect[16,17]. M_s^σ temperature is commonly used to express the austenite stability. When the actual temperature is lower than M_s^σ, the transformation kinetic of γ→α is dominated by stress-assisted nucleation. Otherwise, it is dominated by strain-induced nucleation. Thus, γ→α transformation has the highest rate just at or near M_s^σ temperature[18]. For traditional structural steels, the M_s^σ temperature of γ should be designed near room temperature (25—50 °C) to get a good TRIP effect, which will lead to good toughness for the steel. In order to estimate M_s^σ temperature of γ, Olson-Cohen model was established and widely used in TRIP steels[19,20]. Although many researches about TRIP effect were reported in TRIP steels, few studies focused on the austenite stability design in high Co-Ni secondary hardening steels. In order to figure out the main factor of austenite stability in high Co-Ni secondary hardening steels, three experimental steels were fabricated in this work. The morphology and element distribution of austenite layers were observed, and the austenite stability was analyzed by Olson-Cohen model.

* Corresponding author. Assoc. Prof., Ph.D.
E-mail address: *chizhang@tsinghua.edu.cn* (*C. Zhang*).

Received 6 July 2016; Received in revised form 16 August 2016; Accepted 17 August 2016
Available online 15 February 2017

2. Material and Methods

Three experimental steels with different Ni contents were fabricated and named A12Ni, A8Ni and A5Ni, respectively. The samples studied in this work were taken from the 20 kg ingot, which was fabricated by using an induction melting furnace, without rolling. The samples were taken from the center of the ingots. The main composition of the steels is listed in Table 1, based on the composition of AerMet100 (a commercial high Co-Ni secondary hardening steel)[21]. All the three steels were normalized at 890 °C for 1 h and quenched in oil to room temperature, then immediately transferred to a cryogenic bath, held at −73 °C for 2 h, and finally aged at 482 °C for 5 h, based on the optimum heat treatment process of AerMet100 steel[22].

Table 1
Main composition of experimental steels used in this work (wt. %)

Steel	C	Ni	Co	Mo	Cr	Fe
AerMet100	0.23	11.50	13.50	1.40	3.20	Balance
A12Ni	0.23	11.79	13.24	1.40	3.25	Balance
A8Ni	0.23	8.02	13.64	1.42	3.22	Balance
A5Ni	0.23	4.87	13.50	1.40	3.26	Balance

Samples of the steels were mounted, polished, etched with 5 vol. % nitric acid in ethanol. Six samples were taken from every kind of steel to observe the microstructure. All the microstructure observation was carried out by JEOL JEM2011 (Japan Electron Optics Ltd., Tokyo) at 200 kV. Fracture toughness was measured by standard 25.4 mm-thick compact tension (CT) specimens and every value was tested by five samples.

3. Microstructure Observation and Analysis

Fig. 1 shows the morphology and element distribution of austenite layers in the steels. According to Fig. 1(a—c), nanoscale austenite layers with the width of 3—20 nm formed at the boundary of martensite laths in all the three experimental steels. The morphologies of austenite layers in all the steels were similar, but the element distributions had much difference. Because the sizes of the austenite layers were too small, the experimental results of element distributions were unstable and it was difficult to obtain an accurate value of the mean element content in austenite. However, the change trend of element distributions in austenite could be obtained by experiment. Based on Fig. 1(d), the austenite layer formed in A12Ni had much higher Ni content (30—40 wt. %) than those in other steels, which was similar with the previous results reported in AerMet100[6]. With the decrease of Ni content in the overall composition, the Ni content in austenite layers would also decrease significantly. When the Ni content in the overall composition decreased from 12 to 5 wt. %, the Ni content in austenite layers decreased by nearly 20 wt. % (from about 30 to 10 wt. %). Also, with the decrease of Ni content in the overall composition, the Co content in austenite layers increased slightly.

In order to analyze the element distribution in austenite layers, equilibrium thermodynamic simulation was made by Thermo-Calc software, using TCFE6 database. Fig. 2 shows the simulation results of the element distribution in austenite layers. According to Fig. 2, the decrease of Ni content in the overall composition would not affect the equilibrium content of Ni

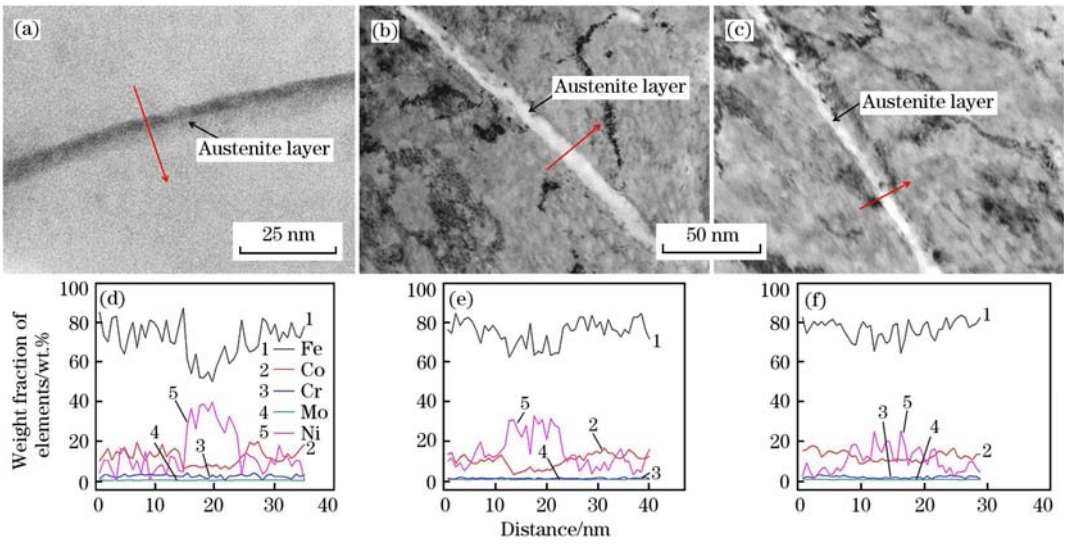

(a) Austenite layers in A12Ni; (b) Austenite layers in A8Ni; (c) Austenite layers in A5Ni; (d) Element distribution of austenite layers in A12Ni; (e) Element distribution of austenite layers in A8Ni; (f) Element distribution of austenite layers in A5Ni.

Fig. 1. Morphologies and element distributions of austenite layers in the steels.

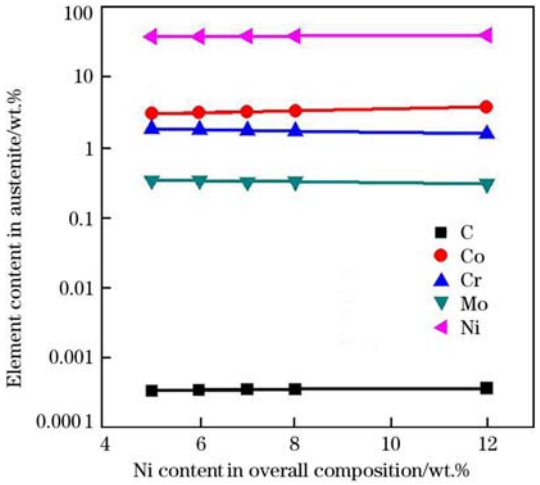

Fig. 2. Equilibrium thermodynamic simulation results of the element distribution in austenite layers.

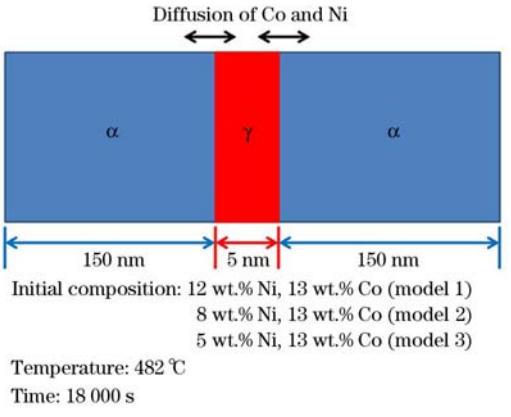

Fig. 3. α-γ-α diffusion kinetic model.

in austenite significantly. When the Ni content in the overall composition decreased from 12 to 5 wt. %, the equilibrium content of Ni in austenite would only decrease from 39.0 to 37.5 wt. %. Also, the equilibrium content of Co in austenite layers would not change significantly. This simulation result seemed inconsistent with experimental results. However, the element diffusion in austenite was a kinetic, instead of an equilibrium process. Because all the steels had relatively higher contents of Ni and Co, the system needed a long time to reach an equilibrium state. It was probable that Ni and Co did not obtain enough time to get the equilibrium content in this system.

In order to simulate the diffusion process of Ni and Co in this system, instead of just obtaining a simulation result in equilibrium state, DICTRA software was used to establish a "α-γ-α" model, as shown in Fig. 3. The width of α and γ was set as 150 and 5 nm, respectively. The initial Ni content in both α and γ was set as 5, 8 and 12 wt. % and the initial Co content is 13 wt. %. The boundary condition was set as the equilibrium content of every element. All the parameters used in this model were obtained from thermo database TCFE6 and dynamic database MOB2 in DICTRA software. The simulation results showed the ideal distribution of Ni and Co in α and γ after aging at 482 °C for 5 h in Figs. 4—6.

Fig. 4 shows the simulation results of element distribution for the model with the initial composition of 12 wt. % Ni and 13 wt. % Co (model 1). The ideal content of Ni near the α/γ interface was similar to the equilibrium value, which was much higher than initial one. During the diffusion process, the Ni and Co contents quickly reached equilibrium value near the interface, then the Ni and Co atoms diffused to the center of γ gradually. After holding at 482 °C for 5 h, the content of Co nearly reached the equilibrium state, but the Ni content at the center of γ was still lower than equilibrium value, which meant that it did not reach the equilibrium state.

Fig. 5 shows the simulation results of element distribution for the model with the initial composition of 8 wt. % Ni and 13 wt. % Co (model 2). Compared with model 1, model 2, which had lower initial content of Ni, had lower diffusion rate for both Ni and Co in γ. Thus, the Ni content at the center of γ was

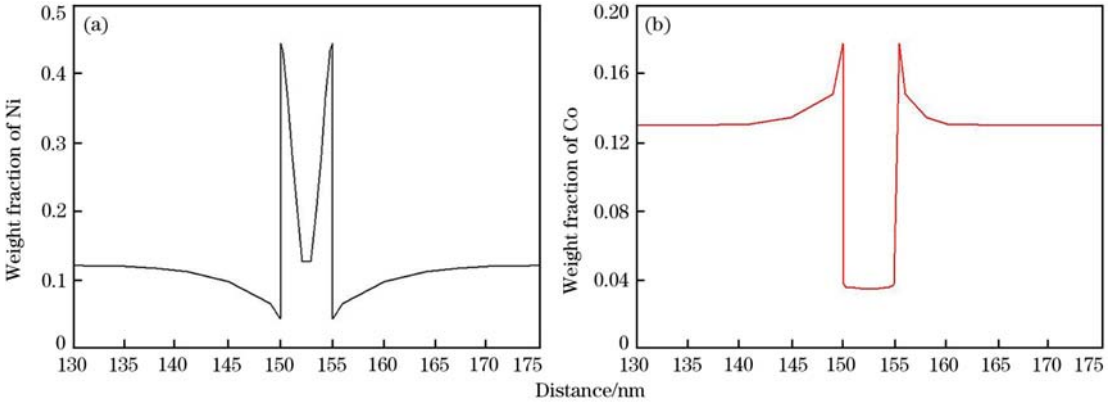

(a) Ni distribution; (b) Co distribution.

Fig. 4. Simulation results of element distribution for model 1 (12 wt. % Ni and 13 wt. % Co).

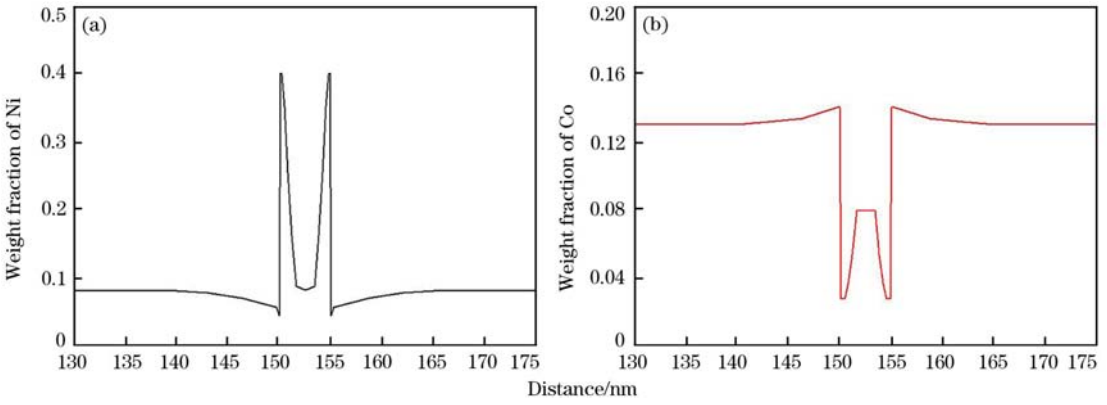

(a) Ni distribution; (b) Co distribution.

Fig. 5. Simulation results of element distribution for model 2 (8 wt. % Ni and 13 wt. % Co).

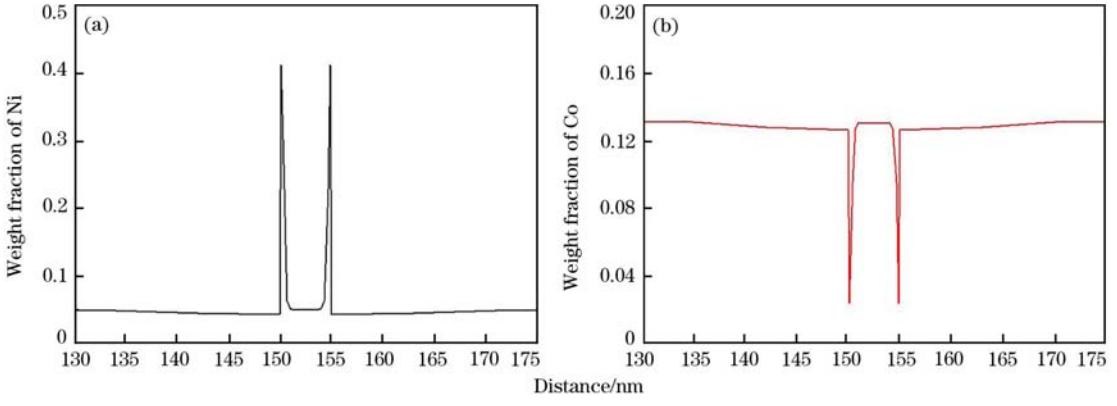

(a) Ni distribution; (b) Co distribution.

Fig. 6. Simulation results of element distribution for model 3 (5 wt. % Ni and 13 wt. % Co).

much lower than equilibrium value. Co also did not get enough time to reach the equilibrium state in γ.

Fig. 6 shows the simulation results of element distribution for the model with the initial composition of 5 wt. % Ni and 13 wt. % Co (model 3). In all the three models, model 3 had the lowest initial content of Ni; thus, it had the lowest diffusion rate for both Ni and Co in γ. Diffusion of Ni and Co could hardly be observed in γ. The contents of Ni and Co remained initial values at the center of γ in the simulation results of model 3. According to the simulation results, the mean content of Ni and Co in γ was estimated by Eq. (1).

$$\overline{w}_i = \frac{\int_{x_0}^{x_f} w_i(x)\,\mathrm{d}x}{x_f - x_0} \tag{1}$$

where, $w_i(x)$ is the weight fraction of element i at x position (i is Ni or Co); x_0 and x_f are the initial and final position of γ, with the value of 150 nm and 155 nm, respectively.

The simulation and experimental results of the mean content of Ni and Co in γ are listed in Table 2. Compared with equilibrium thermodynamic simulation, the results of diffusion kinetic simulation were much closer to experimental results.

Table 2
Simulation and experimental results of the mean content of Ni and Co in austenite layer

Element	Experiment			Simulation		
	12Ni	8Ni	5Ni	12Ni	8Ni	5Ni
Ni	25－40	15－30	10－20	30.8	22.6	13.4
Co	4－6	3－8	8－11	3.7	5.2	10.0

4. Austenite Stability Simulation

Olson-Cohen model was used to simulate the austenite stability. The simulation flow chart is shown in Fig. 7. Based on Olson-Cohen model, M_s^σ temper-

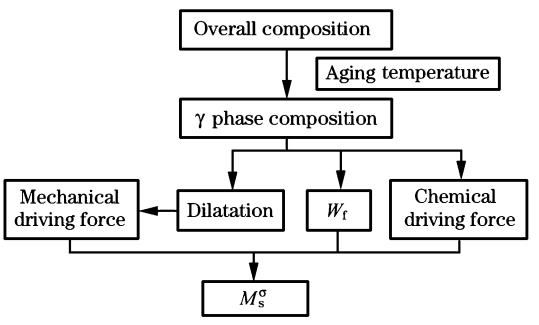

Fig. 7. Simulation flow chart of Olson-Cohen model.

ature was calculated by Eq. (2).

$$\Delta G^{\mathrm{CHEM}}(T)+\Delta G^{\mathrm{MECH}}=-g_{\mathrm{n}}-W_{\mathrm{f}}(T) \quad (2)$$

where, ΔG^{CHEM} and ΔG^{MECH} are chemical and mechanical driving force of γ→α transformation; g_{n} is nuclear potential; and W_{f} is friction work of interface motion. Both ΔG^{CHEM} and W_{f} depended on temperature. Thus, critical temperature, which was equal to M_{s}^{σ}, could be obtained by solving Eq. (2).

4.1. Chemical driving force

The chemical driving force of γ→α transformation could be expressed by Eq. (3).

$$\Delta G^{\mathrm{CHEM}}=G^{\mathrm{BCC}}-G^{\mathrm{FCC}} \quad (3)$$

where G^{BCC} and G^{FCC} are the Gibbs free energy of α and γ. G^{BCC} and G^{FCC}, which depended on γ phase composition and temperature, could be calculated by Thermo-Calc, using SSOL2 database. As analyzed in Part 3, Ni and Co contents could be estimated by diffusion kinetic simulation. For other elements, equilibrium content calculated by Thermo-Calc was used.

4.2. Mechanical driving force

The mechanical work per unit volume done by an applied stress, which assisted the transformation, could be expressed by Eq. (4)[18].

$$W=\tau\gamma_0+\sigma_{\mathrm{n}}\varepsilon_0 \quad (4)$$

where, γ_0 and ε_0 are the resolved shear and normal strains, respectively; and τ and σ_{n} are the resolved shear and normal stresses on the planes in the directions of γ_0 and ε_0, respectively.

After derived by Mohr's circle[23,24], Eq. (4) could be expressed as Eq. (5) for tensile uniform ductility.

$$W=-V_{\mathrm{m}}\sigma\left(\frac{\delta+\sqrt{\delta^2+\gamma_0^2}}{2}\right) \quad (5)$$

where, V_{m} is the molar volume of γ phase; σ is the mean stress; and δ is the dilatation of γ→α transformation.

The dilatation could be expressed by the change of lattice constant, based on Eqs. (6)-(8).

$$\alpha_{\mathrm{BCC}}(\mathrm{nm})=0.287x_{\mathrm{Fe}}+0.283x_{\mathrm{Co}}+0.288x_{\mathrm{Cr}}+0.278x_{\mathrm{Ni}}+0.302x_{\mathrm{Fe}}x_{\mathrm{Ni}} \quad (6)$$

$$\alpha_{\mathrm{FCC}}(\mathrm{nm})=0.360x_{\mathrm{Fe}}+0.354x_{\mathrm{Co}}+0.352x_{\mathrm{Ni}}+0.357x_{\mathrm{Cr}} \quad (7)$$

$$\delta=2\left(\frac{\alpha_{\mathrm{BCC}}}{\alpha_{\mathrm{FCC}}}\right)^3-1 \quad (8)$$

where x_i is the mole fraction of element i.

4.3. Friction work of interface motion

Friction work of interface motion could be divided into two parts: thermal and athermal contributions, as shown in Eq. (9).

$$W_{\mathrm{f}}=W_{\mathrm{athermal}}+W_{\mathrm{thermal}} \quad (9)$$

Thermal and athermal contributions were expressed by Eqs. (10)-(12)[19,20].

$$W_{\mathrm{athermal}}=\sqrt{\sum_i k_{\mu,i}^2x_i}+\sqrt{\sum_j k_{\mu,j}^2x_j}+\sqrt{\sum_k k_{\mu,k}^2x_k}+k_{\mu,\mathrm{Co}}\sqrt{x_{\mathrm{Co}}} \quad (10)$$

$$W_{\mathrm{thermal}}=W_0\left[1-\left(\frac{T}{T_\mu}\right)^p\right]^q \quad (11)$$

$$W_0=W_{\mathrm{Fe}}+\sqrt{\sum_i k_{0,i}^2x_i}+\sqrt{\sum_j k_{0,j}^2x_j}+\sqrt{\sum_k k_{0,k}^2x_k}+k_{0,\mathrm{Co}}\sqrt{x_{\mathrm{Co}}} \quad (12)$$

where, $k_{\mu,i}$ and $k_{0,i}$ are thermal and athermal coefficient for element i; T is absolute temperature; T_μ is the critical temperature, which depended on interfacial rate; p and q are exponent parameters; W_{Fe} is the thermal contribution of Fe; i represents the element C; j represents the element Cr and Mo; and k represents the element Ni.

5. Results and Discussion

Parameters used in Olson-Cohen model is listed in Table 3. Based on the parameters and the simulation results from Thermo-Calc and DICTRA, the M_{s}^{σ} temperature was estimated. Fig. 8 shows the simulation results of M_{s}^{σ} temperature. For the high Co-Ni secondary hardening steel with 12 wt. % Ni, the simulation result of M_{s}^{σ} temperature was about 63 °C, which was relatively closer to the room temperature. When the Ni content in the overall composition decreased from 12 to 8 wt. %, the decrease of Ni content in γ phase led to a significant increase of M_{s}^{σ} temperature. When the Ni content in the overall composition was lower than 7 wt. %, the Ni content

Table 3
Parameters used in simulation

Parameter	Value	Parameter	Value
$k_{\mu,\mathrm{C}}$	3807 J/mol	$k_{0,\mathrm{Cr}}$	3923 J/mol
$k_{\mu,\mathrm{Co}}$	−352 J/mol	$k_{0,\mathrm{Mo}}$	2918 J/mol
$k_{\mu,\mathrm{Ni}}$	172 J/mol	W_{Fe}	836 J/mol
$k_{\mu,\mathrm{Cr}}$	1868 J/mol	g_{n}	6000 J/mol
$k_{\mu,\mathrm{Mo}}$	1418 J/mol	γ_0	0.13
$k_{0,\mathrm{C}}$	21216 J/mol	T_μ	510 K
$k_{0,\mathrm{Co}}$	−724 J/mol	p	0.8
$k_{0,\mathrm{Ni}}$	345 J/mol	q	1.4

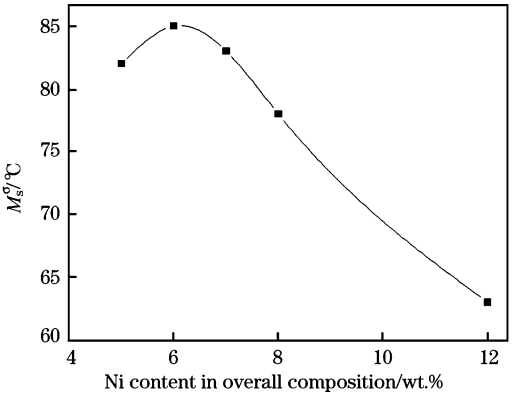

Fig. 8. Simulation results of M_{s}^{σ} temperature.

in γ phase would be lower than 20 wt. %. And the simulation value of M_s^σ temperature would be up to 80 °C, which was about 60 °C higher than room temperature. Higher M_s^σ temperature meant lower austenite stability, which was similar with the common conclusion that lower Ni content could lead to the lower austenite stability. Keeping the austenite stability as a suitable value was the key factor of TRIP effect. When the austenite stability was too high, the γ→α transformation was based on strain-induced nucleation, which would not obtain the highest nucleation rate. Also, when the austenite stability was too low, the γ→α transformation was based on stress-assisted nucleation, which also would not obtain the highest nucleation rate[19,20]. Many different studies reported that a near-room-temperature M_s^σ value represented the suitable value of austenite stability, which was best for obtaining the highest nucleation rate of γ→α transformation and getting the highest toughness of traditional structure steels[19,20]. On the contrary, a far-from-room-temperature M_s^σ value would probably lead to an inefficient TRIP effect, which was disadvantageous for the toughness of steels. In high Co-Ni secondary hardening steels, the TRIP effect was the main factor of the toughness. Also, other factors, such as the solid-solution in austenite, would affect the toughness. However, their effect was much smaller than TRIP effect, because the content of austenite was too small (less than 5%) in high Co-Ni secondary hardening steels.

The K_{IC} value of all three steels studied in this paper was tested to estimate the fracture toughness. The test results are shown in Table 4. It was clear that with the decrease of Ni content, the fracture toughness of the steels decreased significantly. For the steel A12Ni, which had the relatively highest fracture toughness (102 MPa · $m^{1/2}$), the Ni content in γ phase was about 30 wt. % and M_s^σ temperature was about 63 °C. For the steel A8Ni, which had the fracture toughness of 87 MPa · $m^{1/2}$, the Ni content in γ phase was about 20 wt. % and M_s^σ temperature was about 77 °C. For the steel A5Ni, which had the relatively lowest fracture toughness (32 MPa · $m^{1/2}$), the Ni content in γ phase was about 10 wt. % and M_s^σ temperature was about 83 °C. According to the comparison of simulation and mechanical testing results, a basic conclusion could be made that the decrease of Ni content in overall composition was disadvantageous for the fracture toughness of high Co-Ni secondary hardening steels. The diffusion rate of Ni from α to γ was relatively lower in the steels with lower Ni content in the overall composition. Thus, with the same aging temperature and time, the steels with lower Ni content would form the austenite layers with lower Ni content. Low Ni content in γ would lead to the change of austenite stability and finally cause the decrease of fracture toughness.

Table 4
Experimental results of fracture toughness (K_{IC})

Steels	A12Ni	A8Ni	A5Ni
K_{IC}/ (MPa · $m^{1/2}$)	102	87	32

For the newly developed commercial high Co-Ni secondary hardening steels, it was also found that steels with higher Ni content usually had higher fracture toughness (as M54 and AerMet100)[6,25], and low Ni content led to low toughness (as S53)[25]. Thus, for the design of high Co-Ni secondary hardening steels in the near future, the Ni content should be paid much attention. Based on the analysis in this paper, the Ni content in the overall composition of a high Co-Ni secondary hardening steels would not be lower than 8 wt. %, in order to obtain a good fracture toughness.

6. Conclusions

(1) Austenite layers with the width of 3－20 nm were observed in three kinds of high Co-Ni secondary hardening steels. The observation results showed that the Ni content decreased significantly and Co content increased slightly in austenite layers with the decrease of Ni content in the overall composition.

(2) Both equilibrium thermodynamic and diffusion kinetic simulations were used to simulate the element distribution in austenite layer. The simulation results showed that both Ni and Co did not get enough time to reach the equilibrium state in γ after holding for 5 h at 482 °C. The mean content of Ni in γ decreased with the decrease of Ni content in the overall composition.

(3) The decrease of Ni content in overall composition was disadvantageous for the fracture toughness of high Co-Ni secondary hardening steels. Low Ni content in γ would lead to the change of austenite stability and finally cause the decrease of fracture toughness.

Acknowledgment

This work was financially supported by National Basic Research Programs of China (No. 2015CB654802 and No. 2015GB118001) and National Natural Science Foundation of China (Grant No. 51471094). The authors would like to acknowledge the assistance of Olson's group in Northwestern University with the simulation.

References

[1] P. Tao, C. Zhang, Z. Yang, H. Takeda, J. Iron. Steel. Res. Int. 17 (2010) No. 5, 74-78.
[2] W. B. Liu, C. Zhang, Z. X. Xia, Z. G. Yang, J. Nucl. Mater.

455 (2014) 402-406.
[3] Z. X. Xia, C. Zhang, N. Q. Fan, Y. F. Zhao, F. Xue, S. J. Liu, Mater. Sci. Eng. A 545 (2012) 91-96.
[4] G. B. Olson, Mater. Sci. Eng. A 438-440 (2006) 48-54.
[5] G. B. Olson, C. J. Kuehmann, Scripta Mater. 70 (2014) 25-30.
[6] R. Ayer, P. M. Machmeier, Metall. Trans. A 24 (1993) 1943-1955.
[7] C. Wang, C. Zhang, Z. Yang, Micron 67 (2014) 112-116.
[8] C. Wang, C. Zhang, Z. Yang, J. Su, Y. Weng, Mater. Sci. Eng. A 669 (2016) 312-317.
[9] Z. F. Hu, X. F. Wu, Micron 34 (2003) 19-23.
[10] C. Wang, C. Zhang, Z. Yang, J. Su, Y. Weng, Mater. Sci. Eng. A 646 (2015) 1-7.
[11] C. Wang, C. Zhang, Z. Yang, J. Su, Y. Weng, Mater. Des. 87 (2015) 501-506.
[12] G. B. Olson, Acta Mater. 61 (2013) 771-781.
[13] Y. Gao, C. Xu, Z. He, Y. He, L. Li, J. Iron Steel Res. Int. 22 (2015) 48-54.
[14] D. Xu, Y. Liu, J. Li, Q. Meng, P. Li, J. Iron Steel Res. Int. 23 (2016) 138-144.
[15] S. G. Shiri, S. A. J. Jahromi, Y. Palizdar, M. Belbasi, J. Iron Steel Res. Int. 23 (2016) 988-996.
[16] J. Chiang, J. D. Boyd, A. K. Pilkey, Mater. Sci. Eng. A 638 (2015) 132-142.
[17] H. S. Park, J. C. Han, N. S. Lim, J. Seol, C. G. Park, Mater. Sci. Eng. A 627 (2015) 262-269.
[18] G. B. Olson, M. Cohen, Metall. Tran. A 13 (1982) 1907-1914.
[19] G. Ghosh, G. B. Olson, Acta Metall. Mater. 42 (1994) 3361-3370.
[20] G. Ghosh, G. B. Olson, Acta Metall. Mater. 42 (1994) 3371-3379.
[21] J. Li, F. Guo, Z. Li, J. Wang, M. Yan, J. Iron Steel Res. Int. 14 (2007) No. 5, 254-258.
[22] D. Figueroa, M. J. Robinson, Corros. Sci. 52 (2010) 1593-1602.
[23] J. Angeles, J. Sound. Vib. 154 (1992) 556-567.
[24] C. Bellver-Cebreros, M. Rodriguez-Danta, Opt. Commun. 212 (2002) 199-210.
[25] H. Jou, Ultra-high-strength High-toughness Steel, US, CA 2715998 A1, 2009.